Edge-Exfoliated Graphites for Facile Kinetics of Delithiation

Jeong-Seok Park, Myeong-Hee Lee, In-Yup Jeon, Han-Saem Park, Jong-Beom Baek,* and Hyun-Kon Song*

i-School of Green Energy, UNIST, Ulsan 689-798, Korea

ABSTRACT As high rate charge and discharge characteristics of energy storage devices become more important with the market of electric vehicles intensively growing, the kinetics of lithiation or delithiation of electrode materials for lithium ion batteries require enhancement. Graphites, the most widely used anode materials, have a limited power density at high discharge rates, while their alternatives, such as silicon and transition metal oxides, show even inferior rate capability. This work was motivated from an idea of what if the edge opening of graphite was zipped more open to lithium ions in the electrolyte. By edge-selective functionalization, the peripheral *d*-spacing of graphite (d_0) was locally controlled. Larger values of d_0 led to higher capacity especially at high discharge rates. Around 2-fold enhancement of capacity or energy density was achieved at 50C discharge rate from 110 to 190 mAh g^{-1} by exfoliating graphite locally in its edge region. Also, the d_0 dependency of delithiation kinetics confirmed that the electrochemical step of Li^+ influx into or efflux out of the interlayer space of graphite is possibly the rate-determining step of lithiation or delithiation.

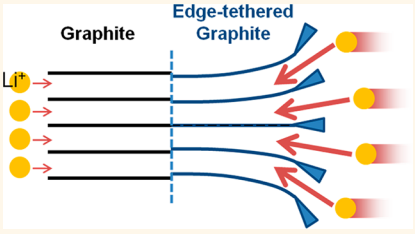

KEYWORDS: graphites · interlayer spacing · nanostructure · lithiation · lithium ion batteries · anodes

Intercalation-based anode materials such as graphites have been widely used for lithium ion batteries.[1,2] As the application target of lithium ion batteries moves from small mobile devices to electric vehicles, high power densities at fast charge/discharge rates have been more and more emphasized. Therefore, kinetics of lithiation and delithiation of graphites need to be improved to satisfy the performance demands of electric vehicles in terms of power density.[3] Novel emerging high capacity anode materials based on conversion[4] or alloying[5] reactions (*e.g.*, transition metal oxides or silicon) deliver even more sluggish kinetics.

The lithiation process of graphite consists of four steps: (C1) introduction of Li^+ into a solid−electrolyte interface (SEI) layer after desolvation; (D2) diffusion of Li^+ through the SEI layer; (E3) intercalation of Li^+ from the SEI layer through the entrance as a gate at the edge site of graphite into the interlayer space between graphene layers; and (D4) Li^+ diffusion along the interspace.[6] A simple hypothesis relating crystallographic parameters of graphite to kinetics of lithiation or delithiation could be followed: the interlayer spacing distance at the entrance (d_0) is responsible for step E3, while the size of crystallites (L) and the interlayer spacing distance at the nonperipheral portion of graphite (d_1) affect the kinetics of step D4. The hypothetical relationship of the first crystallographic parameter d_0 with lithiation kinetics is proven in this work. In terms of the parameter d_1 (not d_0), there have been several reports showing that the larger value of d_1 leads to faster kinetics of lithiation. Potassium-intercalated graphites (KC_8) showed better performances at high rate discharges with d_1 = 0.341 nm (cf. 0.336 nm for bare graphite).[7] Chemical treatment of graphite with H_2SO_4−H_2O_2 enlarged the value of d_1 from 0.3358 to 0.3370 nm, leading to enhanced cyclability at 0.2C with higher capacity.[8,9] However, there were no studies on the effect of localized enlargement of the interlayer spacing especially at edges on lithiation kinetics. One of the reasons for the absence of related research would be the lack of methods controlling the interlayer distance only at the entrance of the interlayer space.

As an alternative approach of graphite-to-graphene exfoliation, edge-selective functionalization of graphite has been reported in a series of papers recently.[10−13] Substituted benzoyl groups were attached to the sp^2 C−H most likely present at the edges of graphite *via* direct Friedel−Crafts acylation. The edge-functionalized groups worked as a molecular wedge exfoliating graphite.

* Address correspondence to jbbaek@unist.ac.kr, philiphobi@hotmail.com.

Received for review September 4, 2012 and accepted November 28, 2012.

Published online November 28, 2012
10.1021/nn3050227

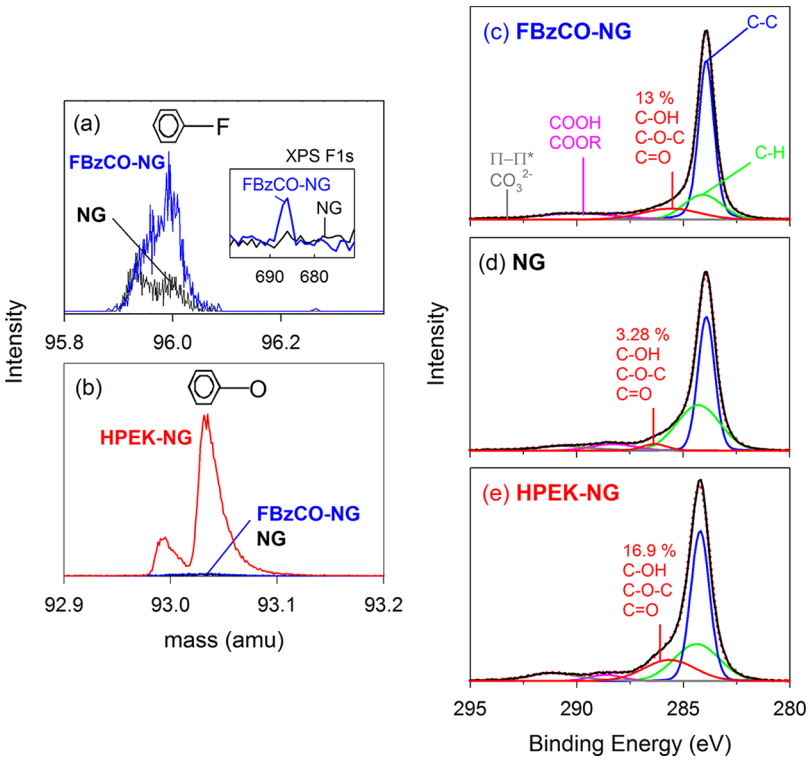

Figure 1. Chemical identification of functional groups edge-tethered to graphites. (a,b) TOF-SIMS of FBzCO-NG (blue) *versus* NG (black) and HPEK-NG (red). The peaks responsible for ^{96}fluorobenzene and ^{93}oxybenzene are indicated in (a) and (b), respectively. F1s XPS spectra are involved in (a) to identify the existence of F in FBzCO-NG. (c–e) C1s XPS spectra of NG and its modified graphites (FBzCO-NG and HPEK-NG). The C1s peaks in (c–e) were fitted with five characteristic peaks assigned to C–C at 283.95 eV, C–H at 284.14 eV (FBzCO-NG) or 284.46 (NG), C═O at 286 eV, and COOR and CO_3^{2-} at higher binding energies.

Unlike conventional Hummer's method to oxidize graphite by acid, there were no serious defect development to disturb crystallinity and electron continuum at the graphitic basal plane. The edge-selective functionalization was implemented in this work not for expanding the interlayer space of graphites in an extreme degree leading to graphene but for increasing the interlayer spacing locally only around the periphery of layers controlling d_0 of graphite. The edge-exfoliated graphites were obtained from macrosize natural graphites (NG; average particle size = ~20 μm). The size of graphitic plates is large enough to provide strong π–π stacking between the graphitic layers. Therefore, the integrity of graphites was maintained even after severe edge exfoliation.

RESULTS AND DISCUSSION

Two different functional groups were introduced selectively at the edges of natural graphite (NG) to control the dimension of d_0 as the primary kinetics-controlling parameter: fluorobenzoyl group (FBzCO–)[10] and hyperbranched poly(ether ketone) group (HPEK–)[13] as a molecular and a macromolecular wedge, respectively. The functionalization was evidenced by identifying the chemical constituents of the functional groups with TOF-SIMS (time-of-flight secondary ion mass spectroscopy) and XPS (X-ray photoemission spectroscopy) (Figure 1): benzoyl-related fragments (fluorobenzene for FBzCO-NG and oxybenzene for HPEK-NG) and carbonyl groups were detected.

In the edge-selectively functionalized NGs (FBzCO-NG and HPEK-NG), the boundary of graphene planes was reported to be exfoliated so that the d_0 dimension increases locally around the edge region ($d_0 > d_{NG}$) (Figure 2a).[10,13] Simultaneously, the stress developed by enlarged d_0 is released in a way to reduce the interspacing dimension of the region far from the boundary ($d_1 < d_{NG}$). The structural change caused by the edge-selective functionalization was confirmed by X-ray diffraction patterns (Figure 2b). With FBzCO-NG wedged by the small molecule and HPEK-NG wedged by the polymeric molecule, the average value of d_{002} decreased from 0.3368 to 0.3361 and 0.3360 nm, respectively, after functionalization (calculated from 2θ of (002) peaks by Bragg's equation, the topmost graph in Figure 2c). Simultaneously, the size of crystallite domain (L) decreased from 28.01 to 24.76 and 23.06 nm (by averaging the values calculated from 2θ of (002) and (004) peaks by Scherrer's equation[14]). The functionalization-induced changes could be interpreted as development of d-spacing distribution. If the distribution were grouped into three categories, d_{002} would result from balancing or averaging the changes of d_0 for the edge or entrance, d_1 far from the periphery, and d_{01} transient between them.

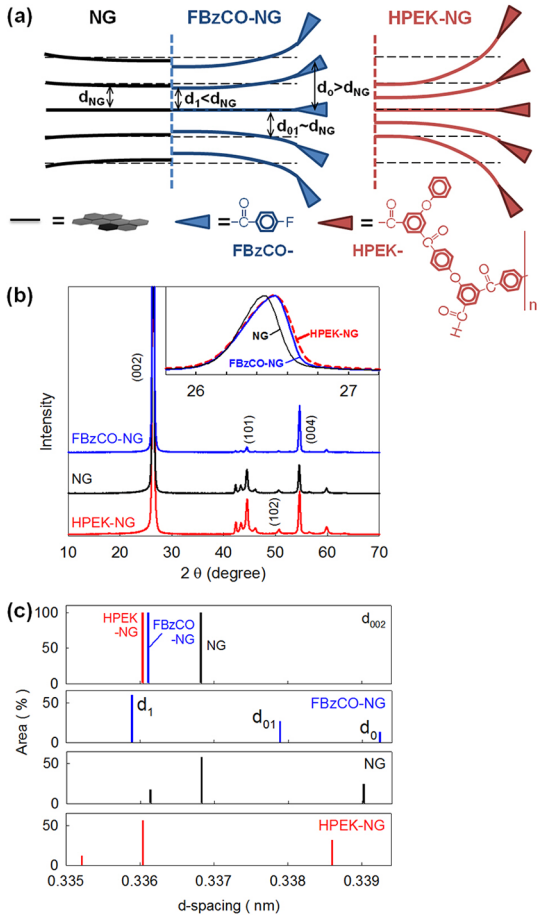

Figure 2. (a) Schematics of layered structures in peripheral region of bare and edge-selectively functionalized natural graphites. The values of *d*-spacing are distributed for all graphites, which were grouped into three phases represented by d_0, d_{10}, and d_1 from surface to bulk; d_{NG} indicates the average value of *d*-spacings of NG, which is equivalent to d_{002} measured by X-ray diffraction. (b) XRD patterns. The (002) peaks were compared in the inset at the same peak intensity. (c) Value of *d*-spacing (d_{002}) calculated from 2θ of (002) peaks and three representative *d*-spacing's (d_0, d_{01}, and d_1) deconvoluted from d_{002}; d_0 is considered as the *d*-spacing of the peripheral region of graphites.

Even if the effects of microstrains caused by nonuniform lattice distortion on peak broadening are negligible with no significant development of strain estimated by the Williamson−Hall equation,[15] the skewness of asymmetric peaks of XRD ($\gamma = E[((X - \mu)/\sigma)^3]$) is another evidence to support the local exfoliation induced by edge-selective functionalization[15,16] (inset of Figure 2b): γ from −2.15 for NG or −1.95 for HPEK-NG to −3.10 for FBzCO-NG (negative for a distribution skewed to the left or left-tailed). Easily inferred is a proportional relationship between the skewness and degree of heterogeneity due to dimensional distribution of the interlayer spacing. The asymmetry of crystallographic peaks is observed in detrital graphites of metamorphic rocks consisting of carbonaceous materials with different stages of conversion to graphite or different crystallinity.[16] The asymmetric peaks can be resolved into multiple symmetric peaks representing their corresponding crystallography.[17] With a simplified assumption that the functionalized graphites consist of three distinguished crystallite phases, the asymmetric peaks were analyzed by d_0, d_{01} and d_1 representing phases (d_0, d_{01}, and d_1 phases) in the intensity *versus* diffraction coordinate ($s = 2 \cos \theta_p \times (\theta - \theta_p)/\lambda$) domain (Figure S1 in Supporting Information). The volume fraction of each phase (x_0, x_{01}, or x_1 with $x_0 + x_{01} + x_1 = 1$) was obtained from the fractional integral intensities of the corresponding subprofiles relative to the overall profile.

The NG at d_{002} = 0.3368 nm was resolved into the main phase of 58% fraction at the same value of spacing (d_{01} = 0.3368 nm) with shorter and longer *d*-spacing phases at d_0 = 0.3390 nm and d_1 = 0.3361 nm in ∼20% fraction each (the third graph in Figure 2c). Even if the macromolecular wedge (HPEK−) was expected to be more effective in terms of local exfoliation than the small molecular wedge (FBzCO−), the extent of local exfoliation of FBzCO-NG was estimated to be larger than that of HPEK-NG. By edge-tethering NG with FBzCO−, the value of d_0 increased slightly with a 0.0002 nm difference, while the center phase was represented by the largely increasing d_{01} with a 0.0011 nm difference (the second graph in Figure 2c). The portion occupied by the inflated phases (d_0 and d_{01} phases) was ∼40.5%. The rest of the constituent phases were characterized by a slightly compressed phase at d_1 = 0.3359 (negative 0.0002 difference from d_1 of NG). The dominant phase in 59.5% is responsible for the decrease in d_{002}. On the other hand, HPEK-NG showed *d*-spacing decrease in all phases, compared with NG and FBzCO-NG. The dominant phase of HPEK-NG was located at d_{01} = 0.3360 nm in more than 56%, which is a smaller value than the smallest dimension d_1 of NG. The reason for the compressed behavior can be found from its calcined control sample. Even after calcining at 900 °C for 2 h in an inert atmosphere to remove the functional group HPEK−, the macromolecular-wedged NG had no change in d_{002}. On the contrary to HPEK-NG, FBzCO-NG showed a reversible recovery to the original *d*-spacing values of NG after removing the edge-tethered moiety (FBzCO−). A possible postulation is that an immoderate exfoliation concentrated on the very near-edge region forces, narrowing the gap between non-edge graphitic plates severely and irreversibly (Figure 2a). The d_0 phase of HPEK-NG would include not only the dimensional increase of extremely localized edge gap ($d_{0,out}$) but also the decrease in near-edge gap ($d_{0,in}$): $d_{0,out} > d_0 > d_{0,in}$. The value of $d_{0,out}$ of HPEK-NG is expected to be larger than d_0 of FBzCO-NG, which is supported by electrochemical impedance spectra (below). As a summary, the extent of local exfoliation or more simply the value of d_0 follows the descending order of FBzCO-NG > NG > HPEK-NG. However, it should be kept in mind that there is every possibility the HPEK-NG

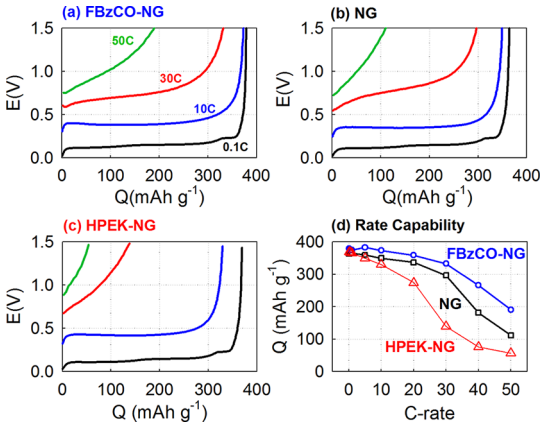

Figure 3. (a−c) Potential profiles of delithiation of FBzCO-NG *versus* NG and HPEK-NG at selected discharge rates. Half cells charged at 0.1C were tested with 1.15 M $LiPF_6$ in EC/DMC (3:7). (d) *C* rate dependency of discharge capacity representing rate capability.

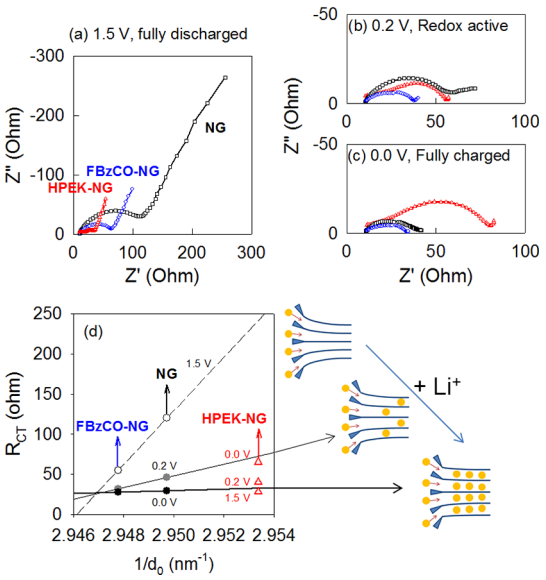

Figure 4. Electrochemical impedance spectra of FBzCO-NG (blue, circle), NG (black, square), and HPEK-NG (red, triangle) at three different biased potentials: (a) 1.5 V (fully delithiated), (b) 0.2 V (partially lithiated), and (c) 0.0 V (fully lithiated). (d) d_0 dependency of resistance (R_{CT}) at three different potentials. The lithiation processes in FBzCO-NG and NG (not HPEK-NG) were schematically described. The same electrolyte as indicated in Figure 3 was used.

contains a small fraction of highly exfoliated edge: $d_{0,out}$ (HPEK-NG) > d_0 (FBzCO-NG) > d_0 (NG) > d_0 (HPEK-NG).

The main point of this work is to reveal the d_0 effects on lithiation/delithiation. With the dimensional information about d_0, therefore, the bare and edge-specifically exfoliated graphites were galvanostatically lithiated and then delithiated in a coin cell configuration with lithium metal (Figure 3) to prove the hypothesis that the d_0 value of graphite is a determining factor for governing kinetics of lithiation/delithiation at least in the step of Li^+ transport between the interlayer space and the SEI layer. At low rates of discharge (*e.g.*, 0.1C or the current at which cells are fully discharged for 10 h), there was no significant difference of capacity between the bare (NG) and edge-specifically exfoliated graphites (FBzCO-NG and HPEK-NG), delivering around the theoretical capacity (372 mAh g^{-1}). The d_0 effects were exhibited more and more distinguishably as the discharge rates increased. By relieving the resistance related to the E3 step of delithiation, FBzCO-NG (d_0 = 0.3392 nm) showed significantly enhanced rate capability especially at high rates, compared with NG: 110 mAh g^{-1} for NG (d_0 = 0.3390 nm) to 190 mAh g^{-1} for FBzCO-NG at 50C. However, HPEK-NG (d_0 = 0.3386 nm) showed inferior rate capability at the same rates such as 50 mAh g^{-1} at 50C. When considering that the d_0 phase of HPEK-NG consists of the extremely exfoliated subphase at the edge region and the relatively compressed subphase at the near-edge region, it is difficult to explain the slow kinetics of HPEK-NG only in terms of d_0. Due to small values of d_{01} and d_1 causing resistance at the D4 step, the inferior rate capability of HPEK-NG can be at least partially explained.

Electrochemical impedance spectra explain the kinetic improvement or deterioration by local exfoliation in a more detailed manner (Figure 4). Impedances of half cells experiencing 50 cycles of charge and discharge were measured at three different biased potentials: 1.5 V (fully delithiated), 0.2 V (partially lithiated), and 0 V (fully lithiated). Highly overlapped and depressed semicircles were observed so that resistances could not be clearly distinguished between C1 and E3 steps mentioned above. The different trends of impedance change were observed with FBzCO-NG and NG *versus* HPEK-NG. The E3 step where the d_0 effect is dominant should be focused with FBzCO-NG and NG, while the D4 step in which the d_{01} or d_1 effect is dominant is emphasized for HPEK-NG. For FBzCO-NG and NG, lower resistances were estimated with graphites of larger d_0 over the whole potential range: FBzCO-NG (57.25 ohm) < NG (117.8 ohm) at 1.5 V in terms of resistance at the fully delithiated states. Degree of lithiation (equivalent to state of charge, SOC) depending on biased potential also decided the impedance of identical graphite. As degree of lithiation goes up, the value of resistance (R_{tot}) as well as its difference between samples (ΔR_{tot}) decreased: R_{tot0} = 106 ohm at SOC = 0 (at 1.5 V) to R_{tot1} = 26.9 ohm at SOC = 1 or 100% (at 0.0 V) with the bare NG; ΔR_{tot0} = 50 ohm and ΔR_{tot1} = 0.8 ohm between the bare and FBzCO-NG. The SOC or potential dependency of impedance can be understood when considering that the interlayer spacing would be enlarged on lithiation with d_1 approaching d_0 (d_{002} = 0.3706 nm for LiC_6[7]), while the difference between d_0 and d_1 would be emphasized with more delithiated graphites (Figure 3d). Therefore, the strong dependency of R_{tot} on d_0 becomes weaker as the degree of lithiation grows higher. The d_0 dependency on resistance can be easily expected from the following

simple equation: $R_{tot} = R_{CT} + R_{others} = Ad_0^{-1} + B$, where R = resistance, subscript tot = total, subscript CT = charge transfer, subscript others = resistance-related processes including C1, A and B = constant. On the assumption that the relationship works with our d_0 varied graphites (Figure 3d), at least in the range of d_0 variation of interest in this work, the regression lines of three different potentials converged on a single intersection point at d_0 = 0.3393 nm. At the values of d_0 larger than that of the intersection point, the resistances of +1.5 V and +0.2 V expected from the regression would be meaningless. Beyond the critical d_0 value, the resistances are expected at the same value independent of applied potentials, or at least resistances obtained at +1.5 V and +0.2 V would not be smaller than that of +0.0 V.

However, the potential dependency of resistance of HPEK-NG is reversed (red triangles at $1/d_0$ = 2.9534 in Figure 4d). As lithiation proceeds from 1.5 to 0.0 V, the R_{tot} increased. The extremely exfoliated opening of edges ($d_{0,out}$) is responsible for the resistance being significantly lower than that of FBzCO-NG and NG at the fully delithiated state at 1.5 V (R_{tot} = 28 ohm for HPEK-NG *versus* 56 ohm for FBzCO-NG and 106 ohm for NG). After the initial Li^+ insertion through the large opening, the additional lithiation feels high resistance due to the significantly reduced interlayer spacing with the rate-determining step moving from E3 to D4. The resistance (which was much lower than that of FBzCO-NG and NG at 1.5 V) increases to a value higher than that of other graphites at 0.0 V: 65 ohm for HPEK-NG *versus* ~28 ohm for others. Therefore, it is concluded that a severe edge exfoliation leads to slow kinetics originating from severe suppression of *d*-spacing in the body of graphites. FBzCO− functionalization can be said to be below a critical point that is the boundary between mild reversible exfoliation and severe irreversible exfoliation.

Even if we tried to isolate the effect of d_0 on electrochemical performances by keeping other characteristics constant, there would be still other variables that have a high possibility of affecting lithiation/delithiation processes. The simultaneous dimensional changes of d_{01} and d_1 in addition to the d_0 change were not negligible. However, this fact does not contrast our conclusion because the better kinetics were obtained with larger d_0 despite the decrease of d_{002}. The chemical composition of the graphite surface should be considered as the main difference between bare and modified graphites. There were no significant differences of impedance between them at the initial open circuit potential just after cells were assembled. During the first lithiation or charging process during which cell potential is shifted from an open circuit potential (practically more positive than 1.2 V *versus* Li/Li^+) to around 0 V *versus* Li/Li^+, various organic molecules existing in the electrolyte are strongly reduced to form a characteristic layer called the solid−electrolyte interface (SEI) layer. The main reduction process practically known to be related to ethylene carbonate (EC) reduction (1.15 M $LiPF_6$ in 3:7 EC/DMC used as an electrolyte for all experiments, where DMC = dimethyl carbonate) was found with all graphites between 0.5 and 0.6 V without any other peaks in curves of d*Q*/d*V* *versus* *V* (where *Q* = capacity and *V* = potential). The Coulombic efficiency of discharge to charge at the first cycle was ~93% for bare and edge-tethered graphites, indicating that the same amount of SEI layer is formed independent of the surface functional groups. The negative effects of the large-sized macromolecular wedge of HPEK-NG (*e.g.*, steric hindrance) do not need to be considered because HPEK-removed HPEK-NG by calcination (the removal of HPEK was confirmed by TOF-SIMS and XPS) showed the same electrochemical characteristics with the same dimension of d_{002} (Figures S2 and S3 in Supporting Information).

CONCLUSIONS

In this work, we proved a feasible hypothesis that enlarged interlayer spacing specifically at the edge (d_0) of graphites leads to facile kinetics of lithiation or delithiation. Without alternatives to graphites or carbons (*e.g.*, conversion or alloying reaction-based materials such as metal oxides[4] and silicon[5]), we believe that nanodimensionally optimized graphite can be beyond conventional anodes of lithium ion batteries in terms of kinetics, satisfying the requirements of lithium ion batteries for electric vehicles.

METHODS

Edge-Selective Functionalization of Graphites. Natural graphites (NG; Mitsubishi Chemical, average particle size = ~20 um) were edge-selectively functionalized with two different moieties, based on direct Friedel−Crafts acylation reactions between graphite and the moieties.[6] The modified graphites were named FBzCO-NG and HPEK-NG after the corresponding functional groups (FBzCO = fluorobenzoyl and HPEK = hyperbranched poly(ether ketone) group). 4-Fluorobenzoic acid and 5-phenoxyisophthalic acid were used as a precursor for the corresponding functional groups of FBzCO-NG and HPEK-NG, respectively. NG and the functional precursor were mixed in the presence of phosphorus pentoxide (P_2O_5) and poly(phosphoric acid) (PPA) under dried nitrogen at 100 °C for 3 h and then heated to 130 °C for 72 h. The composition of the mixture (NG/precursor/P_2O_5/PAA) was 1:4:20:10 g for FBzCO-NG or 2:1:16:60 g for HPEK-NG. The resultant homogeneous mixtures were transferred into distilled water. The solid products were collected by suction filtration, washed with water, Soxhlet extracted with water for 3 days and with methanol for 3 days, and freeze-dried for 48 h.

Compositional and Crystallographic Analysis. Chemical functional groups edge-selectively attached to graphites were identified by a time-of-flight secondary ion mass spectrometry (TOF-SIMS; ION TOF TOF SIMS 5) and a X-ray photoelectron specroscopy

(XPS). The TOF-SIMS measurements were performed at negative secondary ion mode with a pulsed Bi_1^+ cluster ion source (25 kV, 1.02 pA) as a primary beam. K-alpha spectrometer (Thermo Fisher) was used for the XPS measurements with a focused monochromatized Al Kα radiation ($h\nu$ = 1486.6 eV). X-ray diffraction profiles (Rigaku D/MAZX 2500 V/PC X-ray diffractometer with Cu Kα radiation; mean wavelength = 0.15418 nm) were analyzed by the software MDI Jade, which were corrected to remove instrumental broadening by using the instrumental fwhm calibration curve of an external standard (NIST 660b Si).

Electrochemical Analysis. NG, FBzCO-NG, and HPEK-NG were tested as an anodic material of lithium ion rechargeable batteries by using galvanostatic charge/discharge. Coin cells (2016R) were assembled with lithium foil as a counter electrode with 1.15 M LiPF6 in 3:7 v/v ethylene carbonate/dimethyl carbonate (EC/DMC) as electrolyte. Microporous polyethylene film (Tonen, 20 um thick) was used as a separator. A mixture coated on copper foil was used for the anode. It consists of the graphites as an active material, polyvinylidene fluoride (PVdF; KF1100) as a binder, and carbon black (TIMCAL Super P) as a conduction enhancer at a weight ratio of 87:10:3. A slurry of the mixture in *N*-methyl pyrrolidinone (NMP) solvent was coated onto 16 μm thick copper foil, dried at 110 °C for 2 h, and roll-pressed. Areal loading density of active material and thickness of the electrode mixture were fixed at 3 mg cm^{-2} and 40 μm for all samples. Coin cells were assembled in an argon-filled glovebox with less than 1 ppm of oxygen and water. Impedances of half cells were measured at three different biased potentials: 1.5 V (fully delithiated), 0.2 V (partially lithiated), and 0 V (fully lithiated). Sinusoidal signals at 100 kHz to 0.5 Hz were used with 10 mV sinus amplitude. Each measurement was equilibrated at the corresponding biased potential for 5 min before ac stimuli were applied.

Conflict of Interest: The authors declare no competing financial interest.

Acknowledgment. This work was supported by the MEST (WCU:R31-2008-000-20012-0, CRC:2012K001251), MKE (Inter-ER: R0000491, iTRC:NIPA-2012-H0301-12-1009), and POSCO, Korea.

Supporting Information Available: Deconvolution of XRD peaks, compositional and electrochemical characterization of calcined functionalized graphites. This material is available free of charge *via* the Internet at http://pubs.acs.org.

REFERENCES AND NOTES

1. Flandrois, S.; Simon, B. Carbon Materials for Lithium-Ion Rechargeable Batteries. *Carbon* **1999**, *37*, 165–180.
2. Endo, M.; Kim, C.; Nishimura, K.; Fujino, T.; Miyashita, K. Recent Development of Carbon Materials for Li Ion Batteries. *Carbon* **2000**, *38*, 183–197.
3. Kim, T.-H.; Park, J.-S.; Chang, S. K.; Choi, S.; Ryu, J. H.; Song, H.-K. The Current Move of Lithium Ion Batteries towards the Next Phase. *Adv. Energy Mater.* **2012**, *2*, 860–872.
4. Cabana, J.; Monconduit, L.; Larcher, D.; Palacin, M. R. Beyond Intercalation-Based Li-Ion Batteries: The State of the Art and Challenges of Electrode Materials Reacting through Conversion Reactions. *Adv. Mater.* **2010**, *22*, E170–E192.
5. Bang, B. M.; Kim, H.; Song, H.-K.; Cho, J.; Park, S. Scalable Approach to Multi-Dimensional Bulk Si Anodes *via* Metal-Assisted Chemical Etching. *Energy Environ. Sci.* **2011**, *4*, 5013–5019.
6. Zhang, S. S.; Xu, K.; Jow, T. R. Electrochemical Impedance Study on the Low Temperature of Li-Ion Batteries. *Electrochim. Acta* **2004**, *49*, 1057–1061.
7. Tossici, R.; Berrettoni, M.; Rosolen, M.; Marassi, R.; Scrosati, B. Electrochemistry of Kc_8 in Lithium-Containing Electrolytes and Its Use in Lithium-Ion Cells. *J. Electrochem. Soc.* **1997**, *144*, 186–192.
8. Zou, L.; Kang, F. Y.; Li, X. H.; Zheng, Y. P.; Shen, W. C.; Zhang, J. Investigations on the Modified Natural Graphite as Anode Materials in Lithium Ion Battery. *J. Phys. Chem. Solids* **2008**, *69*, 1265–1271.
9. Zou, L.; Kang, F. Y.; Zheng, Y. P.; Shen, W. C. Modified Natural Flake Graphite with High Cycle Performance as Anode Material in Lithium Ion Batteries. *Electrochim. Acta* **2009**, *54*, 3930–3934.
10. Choi, E. K.; Jeon, I. Y.; Bae, S. Y.; Lee, H. J.; Shin, H. S.; Dai, L. M.; Baek, J. B. High-Yield Exfoliation of Three-Dimensional Graphite into Two-Dimensional Graphene-like Sheets. *Chem. Commun.* **2010**, *46*, 6320–6322.
11. Choi, E. K.; Jeon, I. Y.; Oh, S. J.; Baek, J. B. Direct Grafting of Linear Macromolecular Wedges to the Edge of Pristine Graphite To Prepare Edge-Functionalized Graphene-Based Polymer Composites. *J. Mater. Chem.* **2010**, *20*, 10936–10942.
12. Bae, S. Y.; Jeon, I. Y.; Yang, J.; Park, N.; Shin, H. S.; Park, S.; Ruoff, R. S.; Dai, L. M.; Baek, J. B. Large-Area Graphene Films by Simple Solution Casting of Edge-Selectively Functionalized Graphite. *ACS Nano* **2011**, *5*, 4974–4980.
13. Jeon, I. Y.; Choi, H. J.; Bae, S. Y.; Chang, D. W.; Baek, J. B. Wedging Graphite into Graphene and Graphene-like Platelets by Dendritic Macromolecules. *J. Mater. Chem.* **2011**, *21*, 7820–7826.
14. Langford, J. I.; Wilson, A. J. C. Scherrer after Sixty Years: A Survey and Some New Results in the Determination of Crystallite Size. *J. Appl. Crystallogr.* **1978**, *11*, 102–113.
15. Unga, T. Strain Broadening Caused by Dislocations. *Adv. X-Ray Anal.* **1996**, *40*, 612.
16. Wang, G. F. Carbonaceous Material in the Ryoke Metamorphic Rocks, Kinki District, Japan. *Lithos* **1989**, *22*, 305–316.
17. Ungar, T.; Mughrabi, H.; Rönnpagel, D.; Wilkens, M. X-ray Line-Broadening Study of the Dislocation Cell Structure in Deformed [001]-Orientated Copper Single Crystals. *Acta Metall.* **1984**, *32*, 333–342.